

# An Improved Double Closed Loop Control Strategy for Air Plasma Cutting Converter

**Abstract.** A double closed loop control strategy composed of inner voltage-loop and external current-loop with a current-reference feedforward link was proposed based on the output characteristic of an air plasma cutting converter (APCC) with non-contact arc ignition. An equivalent mathematical model of the APCC was presented and a controller was designed via frequency domain analysis. Experiments verified that the proposed control strategy showed excellent dynamic and static performance, which significantly improved the arc ignition and the robustness against load disturbance.

**Streszczenie.** Przedstawiono strategię sterowania konwertera do cięcia plazmowego z podwójną pętlą złożoną z wewnętrznej pętli napięcia i zewnętrznej prądowej. Przedstawiono model matematyczny i projekt z analizą w dziedzinie częstotliwości. Obiekt sprawdzono eksperymentalnie. (Ulepszona strategia sterowania konwertera do cięcia plazmowego)

**Keywords:** air plasma cutting converter; double closed loop; phase-shift full-bridge; arc ignition process.

**Słowa kluczowe:** cięcie plazmowe, podwójna pętla sterowania, zapłon łuku.

## Introduction

Air plasma cutting process is becoming more and more popular in the metal fabrication industry for its advantages in efficiency and economy. Usually, phase-shift full-bridge (PSFB) ZVS converter is chosen as the main circuit of the air plasma cutting converter (APCC), and non-contact arc ignition is introduced to minimize the scathe of the plasma torch. What's more, the PSFB converter can isolate the plasma torch with the grid and realize ZVS simply with its parasitic parameters, which will lead to high power rating and high efficiency [1, 2]. The APCC has a steep output characteristic, where the no-load voltage is usually higher than 150V for the convenience of generating small plasma arc during arc igniting, while it works as a current source in the cutting process, and the output current is adjustable to fit different workpieces[3].

A credible controller and rational parameters must be designed for the APCC if the non-contact arc ignition is introduced, as they should guarantee the dynamic response when the APCC commutates from voltage mode to current mode. In addition, constant no-load voltage and cutting current should be regulated accurately in the steady state [4-6]. Presently, most of the controllers for APCC include only single closed loop, either single current loop, or voltage loop and current loop parallel-connected with selector switch, and other improved control methods [7-9]. For the first one, the uncontrolled output voltage is bad for arc ignition. The second one is the betterment of the first one, the constant output voltage is helpful to form the plasma arc, however the switching point between the two closed loops is hard to decide and the serious EMI during arc igniting may disturb the controller—the switching process may execute on and off, even shut down the whole system. A peak current is involved in a double closed loop controller in [9], the peak current from the primary of the transformer is introduced in the inner current loop and the average arc current is detected to the outer current loop, which can control the current through the power switches periodically, but hardly improved the dynamic performance.

In this paper, a double closed loop control strategy is proposed, which is composed of inner voltage-loop and external current-loop with a current-reference feed forward link. The outer loop will be saturated to the limit value as the reference of the inner voltage loop. The outer current loop will desaturate soon after the arc igniting and the interaction of both loops generates the phase angle for the PSFB. This control strategy has excellent dynamic performance and

well suit for non-linear system, what's more, it improved the arc ignition process significantly and experiments verified the proposed control strategy.

## Modelling for APCC

The main circuit of the APCC is shown in Fig.1, with a PSFB in the front end following by a full bridge rectifier.  $R_a$ ,  $C_a$  and the high frequency high voltage source (HFHV, about 1 MHz/7 000 V) are used for arc igniting. S1 and S2 are turned off, and the HFVF is out of work under no-load condition. When cutting process is pulsed-on, S1 and S2 are turned on and the HFHV is series-connected between the nozzle and the tungsten cathode via a coupling boost transformer, which punctures the air between them and forms a horizontal small plasma arc. At the same time, the no-load voltage generate an arc current via  $R_a$ , which can be sprayed out to the workpieces by the compressed air through the nozzle, and the APCC will commutate to current mode synchronously. The key parameters of the system are listed in Table 1.

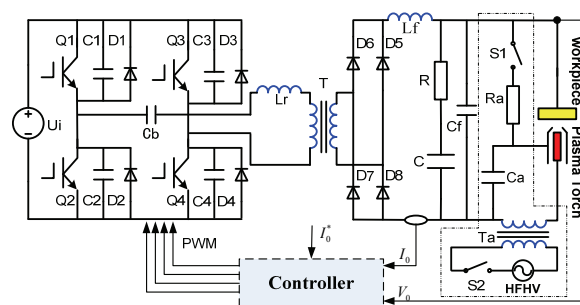


Fig.1. Main circuit of air plasma cutting converter

Table 1. Key parameters of the system

Parameters	Value
Switch frequency: $f_s$	20 kHz
Turn ratio of transformer: $n$	1.8 : 1
Input voltage: $U_i$	400 - 600 V
Resonant inductor: $L_r$	38 $\mu$ H
Output inductor: $L_f$	90 $\mu$ H
Output capacitor: $C_f$	3 $\mu$ F

Some hypotheses are drawn before the analysis work: 1) all the power semiconductor devices are ideal; 2) all the inductors, capacitors and transformer are ideal. Then the model of PSFB can be evolved from the small signal model

of buck converter by modifying the duty cycle  $D$  [10]. In fact, the APCC must change from voltage mode to current mode in cutting process and wide output current range is required also, restricting the veracity and reliability of the small signal model for APCC. Nevertheless, this defect can be obviated by elaborating the controller. Usually, resonant inductor is introduced to realize ZVS for the lagging leg of PSFB while certain duty cycle will vanish. The efficient duty cycle can be defined as

$$(1) \quad D_{eff} = D - \Delta D$$

Where  $D$  is the duty cycle generated by the controller, and

$$(2) \quad \Delta D = \frac{2nL_r}{U_i T_s} \left[ 2I_f - \frac{U_o}{L_r} (1-D) \frac{T_s}{2} \right]$$

Wherein,  $\Delta D$  is the lost duty cycle;  $T_s$  is the switching time;  $I_f$  is the current of the output inductor. The effect of the lost duty cycle can be converted to series-connected impedance with the output inductor as shown in Fig.2. Where  $R_o$  is the equivalent resistance of the arc current, and the impedance is described as

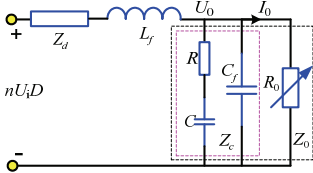
$$(3) \quad Z_d = 4n^2 L_r f_s$$


Fig.2. Equivalent circuit of PSFB in APCC

According to Fig.2, the transfer function from  $D$  to  $U_o$  is given by

$$(4) \quad G_{vd}(s) = \frac{nU_i Z_o}{sL_r + Z_o + Z_d}$$

Where

$$(5) \quad \begin{cases} Z_c(s) = \left( \frac{1}{sC} + R \right) // \frac{1}{sC_f} \\ Z_o(s) = Z_c(s) // R_o \end{cases}$$

$C_f$  is a high frequency capacitor that can eliminate the interferential signal during the cutting process, and its value is very small comparing to  $C$  in the  $RC$  branch. Therefore

$$(6) \quad s = j2\pi f \gg \frac{1}{RC_f}$$

And the effect of  $C_f$  can be neglected in approximation, hence formula (4) can be rewritten as

$$(7) \quad G_{vd}(s) = nU_i (sCR + 1) / \left\{ L_r C \left( \frac{R}{R_o} + 1 \right) s^2 + [CZ_d \left( \frac{R}{R_o} + 1 \right) + CR + \frac{L_r}{R_o}] s + \left( \frac{Z_d}{R_o} + 1 \right) \right\}$$

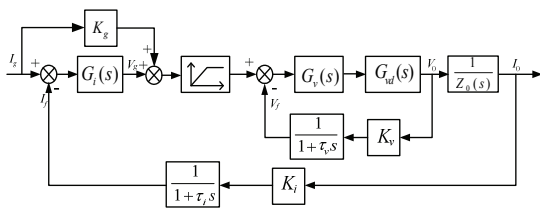


Fig.3. Control block of the proposed control strategy

## Design of Controller

### A. Controller Strategy

The proposed control block is shown in Fig.3. Both of the compensators in voltage and current loops are PI links [11-13], and low-pass filters (first-order inertia link) are adopted to smooth the signals getting from the APCC with serious noise.

$G_i(s)$  and  $G_v(s)$  are current and voltage compensators respectively;  $K_g$  is the feed forward link;  $K_i$  and  $K_v$  are the output current and voltage sensor coefficients respectively;  $\tau_i$  and  $\tau_v$  are the inertia time constants of the sampling circuits for the output current and voltage respectively. Fig.4 shows the new control block after rearranging the control block in Fig.3, thus the transfer function of the whole system can be arranged as follow

$$(8) \quad G_{closed}(s) = \frac{G_v(s)G_{vd}(s)[G_i(s) + K_g]G_o(s)}{1 + G_v(s)G_{vd}(s)H_v(s) + G_v(s)G_{vd}(s)H_i(s)G_o(s)}$$

where  $H_v(s) = K_v / (1 + \tau_v s)$ ;  $H_i(s) = K_i / (1 + \tau_i s)$ ;  $G_o(s) = 1/R_o(s)$ ;  $K_g$  is contained in the numerator of  $G_{closed}(s)$ , hardly affects the stability of the system but shares the burden of the current controller and accelerates the response speed. Actually,  $G_i(s)$  only needs to supply the small signal while the feed forward link provides the entire big signal of the current reference. Consequently, the compensators can design to fit any load conditions without changing parameters.

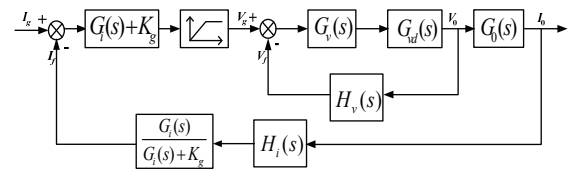


Fig.4. Equivalent control block of the double closed loop

### B. Equivalent Resistance of the Arc Current

The arc ignition generated plenum plasma between the nozzle and the tungsten cathode before the small plasma arc being sprayed out, thus the voltage between the nozzle and workpiece equates to the no-load voltage with the length of the plasma arc is  $L_1$ . The plasma arc spans from the cathode to the workpiece in the cutting process with the length of plasma arc is  $L_2$ . The voltage of the plasma arc can be written as

$$(9) \quad U_{ARC} = K_1 I_{ARC} + 20 + K_2 L_2$$

Where  $K_1$  is a small constant relative to arc current,  $K_2$  is a constant relative to the length of plasma arc. A plasma torch TYL80P is applied and the parameters are listed in Table 2.

Table 2. Parameters related to the cutting process

Parameter	$L_1$ [mm]	$L_2$ [mm]	$K_1$ [ $\Omega$ ]	$K_2$ [V/mm]
Value	2.5	7.5	0.35	9.6

From Table 2 and formula (9), the equivalent resistance  $R_{ARC} = U_{ARC}/I_{ARC} = 0.45 \Omega$  during the arc igniting process and this will be the worst condition for the controller. Thus, the controller should be effective covering the load resistance from  $0.45 \Omega$  to infinite (no-load).

### C. Design of Inner Voltage Loop

The inner voltage loop must be designed to obtain fast response to the output voltage, which can reignite quickly soon after flameout at whiles in cutting process, also it can react rapidly to disturbance from the grid. The bandwidth

frequency is relative high,  $K_v = 1$  and  $\tau_v = 0.5\text{ms}$ .  $R_o$  is  $\infty$  under no-load condition, thereby the transfer function of the voltage open loop is

$$(10) \quad G'_{vd}(s) = G_{vd}(s) \frac{1}{1 + \tau_v s} \Big|_{R_o = \infty}$$

The bode diagram of  $G'_{vd}(s)$  is shown in Fig.5, where the amplitude gain in the low-frequency segment is big enough but the cut-off frequency is  $2.035 \times 10^5 \text{ rad/s}$  before rectified, which is bigger than the switch frequency and even magnify noises from the switches. Generally, the expectant cut-off frequency is set to be  $1/20$  of the switching frequency, thus  $\omega_c = 6280 \text{ rad/s}$  with amplitude gain  $L(\omega_c)$  is  $37.6 \text{ dB}$ .

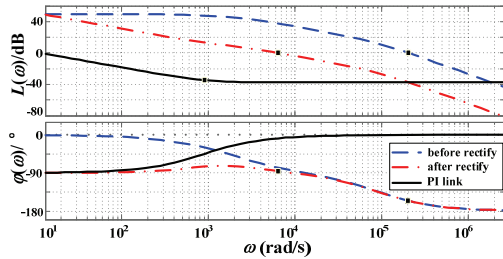


Fig.5. Bode diagram of voltage loop

The PI link is employed in the controller and defined as

$$(11) \quad G_v(s) = \frac{K_p s + K_I}{s}$$

In order to eliminate the second harmonic transmitted from the grid, the corner frequency of PI link is restricted by

$$(12) \quad \omega_m > 2\pi \cdot 2f_{grid}$$

Where  $\omega_m = 900 \text{ rad/s}$  is selected, then

$$(13) \quad \begin{cases} -20 \lg K_p = L(\omega_c) \\ K_I = K_p \omega_m \end{cases}$$

Fig.5 shows the bode diagrams, including the one before rectifying, after rectifying and the designed PI link, where the cutting frequency reduced to the designed value with the phase margin and amplitude margin are improved markedly.

#### D. Design of Outer Current Loop

The main object of the outer current loop is to set up the arc current quickly and limit its overshoot to avoid aggravating the current stress of the rectify diodes. Single-point discharge may take place and anode speckles formed if the arc current is too big during spraying out from the nozzle, which may result in failed arc igniting. The load condition is worst as it changes dramatically during the period of arc igniting, thus we consider  $R_o = 0.45 \Omega$  when designing the current compensator and the open loop transfer function without controller is

$$(14) \quad \begin{aligned} G_{id}(s) &= [G_i(s) + K_g] G_{vd}^{close}(s) \frac{1}{1 + \tau_i s} \frac{1}{R_o(s)} \frac{G_i(s)}{G_i(s) + K_g} \\ &= G_i(s) G_{vd}^{close}(s) \frac{1}{1 + \tau_i s} \frac{1}{R_o(s)} \Big|_{R_o = 0.45 \Omega} \end{aligned}$$

Wherein,  $K_i = 1$ ,  $\tau_i = 1\text{ms}$ , however, the high order system is difficult to commentate with theorems in frequency domain, thereby order-reduction arithmetic is introduced [14]. The transfer function before order-reduction can be rewritten as

$$(15) \quad G_{id}(s) = \frac{b_1 s^m + b_2 s^{m-1} + \dots + b_m s + b_{m+1}}{a_1 s^n + a_2 s^{n-1} + \dots + a_n s + a_{n+1}}$$

Where  $b_i (i = 1, 2, \dots, m+1)$ ,  $a_i (i = 1, 2, \dots, n+1)$  are constants, and its order-reduced expression is

$$(16) \quad G'_{id}(s) = \frac{\beta_1 s^r + \beta_2 s^{r-1} + \dots + \beta_{r+1}}{\alpha_1 s^k + \alpha_2 s^{k-1} + \dots + \alpha_k s + \alpha_{k+1}}$$

Where  $\alpha_i (i = 1, 2, \dots, r+1)$ ,  $\beta_i (i = 1, 2, \dots, k+1)$  are constants, and  $k < n$  must be satisfied for a stable system.  $G_{id}(s)$  can be described with Maclaurin series, and its coefficients are

$$(17) \quad c_i = \frac{1}{i!} \frac{d^i G_{id}(s)}{ds^i} \Big|_{s=0} = -CA^{-(i+1)}B, \quad i = 0, 1, \dots$$

Where  $A$ ,  $B$ ,  $C$  are the coefficient matrixes in the state equation of  $G_{id}(s)$ . In order to maintain the consistency after order-reduction, equation (18) must be satisfied

$$(18) \quad \begin{bmatrix} c_r & c_{r-1} & \dots & \dots \\ c_{r+1} & c_r & \dots & \dots \\ \vdots & \vdots & \ddots & \vdots \\ c_{k+r-1} & c_{k+r-2} & \dots & c_r \end{bmatrix} \begin{bmatrix} \alpha_k \\ \alpha_{k-1} \\ \vdots \\ \alpha_1 \end{bmatrix} = - \begin{bmatrix} c_{r+1} \\ c_{r+2} \\ \vdots \\ c_{k+r} \end{bmatrix}$$

Where  $\alpha_i$  can be figure out by submitting (17) in (18), and  $\beta_i$  can be obtained by

$$(19) \quad \begin{bmatrix} \beta_{r+1} \\ \beta_r \\ \vdots \\ \beta_1 \end{bmatrix} = \begin{bmatrix} c_0 & 0 & \dots & 0 \\ c_1 & c_0 & \dots & 0 \\ \vdots & \vdots & \ddots & \vdots \\ c_r & c_{r-1} & \dots & c_0 \end{bmatrix} \begin{bmatrix} 1 \\ \alpha_k \\ \vdots \\ \alpha_{k-r+1} \end{bmatrix}$$

The relative-order of  $G_{id}(s)$  is second, so  $k-r=2$  should be established. The approximation model is veracious enough when  $r=1$  and  $k=3$ , so the current open-loop transfer function without compensator can be derived by matrix (18) and (19)

$$(20) \quad G'_{id}(s) = G_{id}(s) \Big|_{6 \rightarrow 3}^{4 \rightarrow 1} = \frac{\beta_1 s + \beta_2}{\alpha_1 s^3 + \alpha_2 s^2 + \alpha_3 s + \alpha_4}$$

Fig.6 shows the bode diagrams of  $G_{id}(s)$  and  $G'_{id}(s)$ , where the curves superpose well especially in the segment below  $1.5 \times 10^4 \text{ rad/s}$ , which testify the order-reduction model.

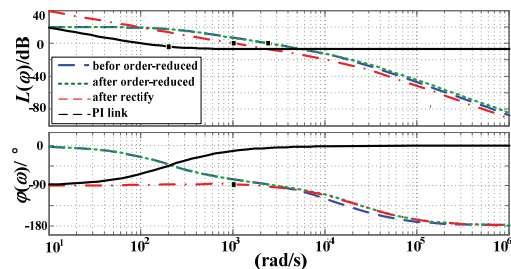


Fig.6. Bode diagram of current loop

Like the aforementioned analysis, the current PI link is

$$(21) \quad G_i(s) = \frac{K'_p s + K'_I}{s}$$

Setting the cut-off frequency of the current loop  $\omega'_c = 1000 \text{ rad/s}$  and the corner frequency  $\omega'_m = 200 \text{ rad/s}$ , then

$$(22) \quad \begin{cases} -20 \lg K'_p = L(\omega'_c) \\ K'_I = K'_p \omega'_m \end{cases}$$

Thereby, the PI link can be figure out based on the order-reduced system. Fig.6 shows the bode diagram, where the cutting frequency reduce to the anticipant value with moderate phase margin and amplitude margin and good performance is obtained.

### E. Design of Feed Forward Link

From formula (8) and Fig.4, we can see that the loop gain increased with  $K_g$  on the steady state in cutting process, and

$$(23) \quad K_g I_g + U_g = U_f = I_f R_o$$

As pointed out foregoing,  $U_g$  (the output of  $G_i(s)$ ) just offers a small signal, thus we select  $U_g = 1/6 U_f$ , then

$$(24) \quad K_g = 5I_f R_o / 6I_g$$

However, the equivalent resistance during the arc ignition is rather small and the output current reaches its peak value  $I_{fmax}$ , which make instantaneous minus  $U_g$ , thus

$$(25) \quad U_g = K'_p (I_g - I_{fmax})$$

Therewith, the output voltage reduces to its minimum because of the discharge in the arc igniting circuit. Thus, the input signal of inner compensator must be elevated quickly while increasing the output of the feed forward link is the most efficient choice. According to (23)-(25), inequation about  $U_g$  can be established as

$$(26) \quad \frac{K'_p (I_{fmax} - I_g) + I_{fmax} R_{ARC}}{I_g} < K_g < \frac{5I_f R_{o\min}}{6I_g}$$

Where  $R_{o\min}$  is the minimum equivalent resistance of the arc current in cutting process, and  $I_f = I_g$  found on the steady state.  $I_{fmax}$  is related to the main circuit and the plasma torch, and we have  $I_{fmax} = 1.5I_g$  in this system, thereby, (26) can be rearranged as

$$(27) \quad 0.5K'_p + 1.5R_{ARC} < K_g < 5R_{o\min} / 6$$

Therefore, the overall closed loop control system can be optimized with equation (27).

### Simulation and Experiment of APCC

Matlab simulation work is carried out via the foregoing analysis. Fig.7 shows the trends of frequency characteristic, and Fig.8 shows the unit step response curves when the load resistance changes from  $0.45 \Omega$  to  $3 \Omega$ , respectively. The cut-off frequency changes little with sufficient phase margin, where the amplitude gain is higher than 50 dB in the low-frequency segment and lower than -50dB in the switch frequency, which attains perfect performance under all the load conditions. Fig.9 shows the unit step response curves when  $R_o = 1.5 \Omega$  by changing  $K_g$  from 0.9 to 1.2, and the settling time devalued by more than 20ms.

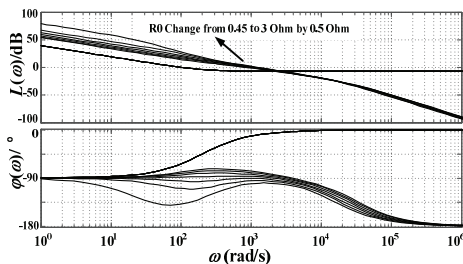


Fig.7. Frequency characteristic curves of system in current mode

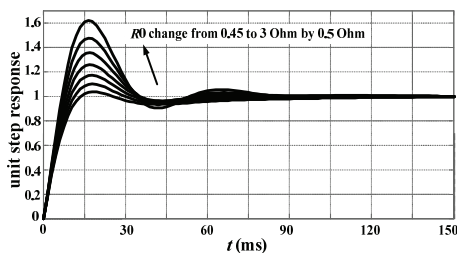


Fig.8. Step response curves in current mode when changing  $R_o$

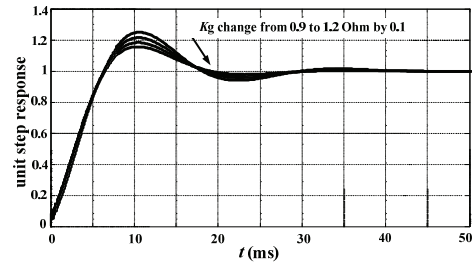


Fig.9. Current step response curves of system when changing  $K_g$

Fig.10 shows the output voltage and current waveforms with  $1.5 \Omega$  arc current resistance; besides the arc igniting resistance is  $0.45 \Omega$  by lasting 5ms. The arc ignition is triggered 60ms after the no-load voltage is setting up. We can see that the peak of the arc current is accredited, and the settling time is about 20ms after turning off the arc ignition branch. The reference of current reduces to 60A at 100ms and changes back to 80A after 60ms, where the current levels off quickly with only 5% overshoot and high steady-state precision. Fig.11 shows the transformation when the load resistance reduces from  $1.5 \Omega$  to  $1.2 \Omega$ , where the controller suppresses the load disturbance effectually.

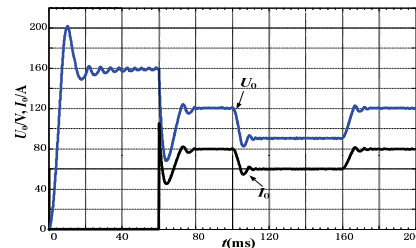


Fig.10. Output waveforms when changing the reference current

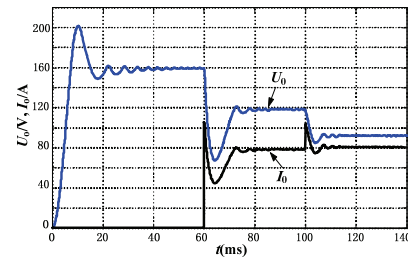


Fig.11. Output waveforms when changing the load resistance

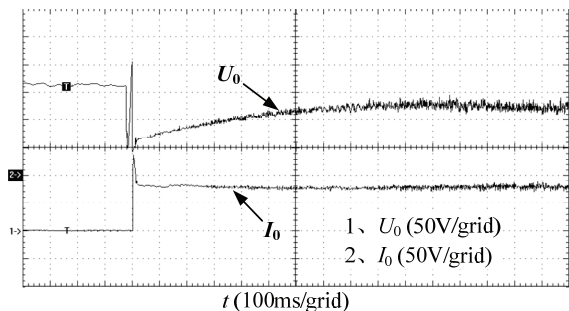


Fig.12. Output waveforms when cutting with 80A current

A 12-kW prototype is fabricated with no-load voltage at 160V and adjustable output current from 45A to 80A. According to equation (27), we can get  $0.9 < K_g < 1.25$ , and  $K_g = 1.2$  is drawn in this system. Fig.12 shows the output current and voltage waveforms when cutting a 15mm mild steel with 80A current. There is no current before the arc current spraying out, and the outer compensator is saturated. During arc igniting process, the HFHV and arc

ignition circuit discharged and the output voltage dropped, which excited the controller put out the maximal duty cycle to maintain a high arc voltage, thus increasing the plasma in the nozzle. A peak current of 130A desaturate the current loop, and a moderate voltage can guarantee the success of the arc ignition. In a word, the rapid response of voltage loop can hold the plasma and the current loop can ensure a constant arc current, while the cooperation of both loops insure the successful arc igniting process.

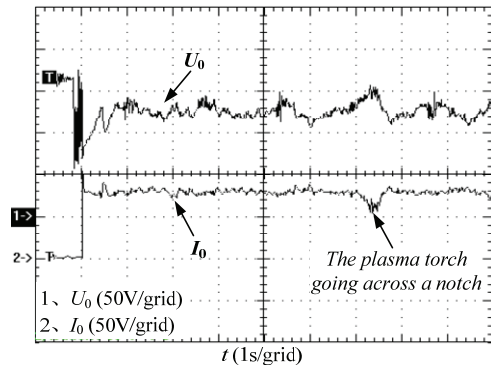


Fig.13. Output waveforms when cutting rough workpieces

Fig.13 shows the output waveforms when cutting rough workpieces. When the plasma torch going across a notch, the plasma jet stretched with the equivalent resistance increased, which result in a valley current and a peak voltage, however, the controller regulate the arc current quickly with excellent robustness and reliability.

### Conclusion

A mathematic model is presented for the APCC and a double closed loop controller is designed. It has merits as follow: (1) rapid response for inner voltage loop, which can restrain the disturbance form the grid and set up the voltage quickly to enhance the ignition process, (2) the outer current loop ensure excellent dynamic and static performance in the full range of the load. Experiments testify that the proposed control strategy assured the reliability of arc igniting and the arc current is stable with steady plasma jet, little sparks and smooth kerfs.

### Acknowledgements

The authors would like to thank financial supports provided by National Basic Research Program of China (973 Program) and its project number is 2010CB227206.

### REFERENCES

- [1] Gwan-Bon Koo, Gun-Woo Moon, Myung-Joong Youn, New Zero-Voltage-Switching Phase-Shift Full-Bridge Converter With Low Conduction Losses, *IEEE Trans. Ind.Electron.*, 52(2005), No.1, 228-235.
- [2] Wu Xinke, Xiaogao Xie, Junming Zhang, et al. Soft Switched Full Bridge DC-DC Converter With Reduced Circulating Loss and Filter Requirement, *IEEE Trans. Power Electron.*, 22(2007), No.5,1949-1955.
- [3] Zhu Guorong, Liu Zhao, Li Xun, et al. The Multi-functional Arc Welding/Cutting Inverter Based on PS-FB-ZVZCS, *IEEE Conference on Industrial Electronics and Applications*, 2007, 1912-1916.
- [4] Jose Gonzalez-Aguilar, Cecilia Pardo Sanjurjo, Antonio Rodriguez-Yunta, et al. A Theoretical Study of a Cutting Air Plasma Torch, *IEEE Trans. Plasma Science.*, 27(1999),No.1, 264-271.
- [5] Ramakrishnan S., Gershenzon M., Polivka F., et al. Plasma Generation for the Plasma Cutting Process, *IEEE Trans. Plasma Science*, 25(1997), No.5, 937-946.
- [6] Schavemaker P. H., Van der Sluis L., An Improved Mayr-type Arc Model Based on Current-zero Measurements, *IEEE Trans. Power Delivery*, 15(2000), No.2, 580-584.
- [7] Sanajit N., Jangwanitert A., Improved Performance of a Plasma Cutting Machine Using a Half-bridge DC/DC Converter, *International Conference on Robotics and Biomimetics*, 2008, 1601-1606.
- [8] Chae Y. M., Jang Y., Jovanovic M. M., et al. A Novel Mixed Current and Voltage Control Scheme for Inverter Arc Welding Machines, *IEEE Applied Power Electronics Conference and Exposition*, 2001, 308-313.
- [9] Fang Chenfu, Yin Shuyan, Hou Runshi, et al. Double Close Loops Control System of Peak Current Mode of Inverter Arc Welding Power Supply, *Transactions of The China Welding Institution*, 26(2005), No.10, 14-18.
- [10] Vlatko V., Juan A. S., Raymond B. R., et al. Small-signal Analysis of the Phase-shifted PWM Converter, *IEEE Trans. Power Electron.*, 7(1992), No.1, 128-135.
- [11] Jia Deli, You Bo, Zhang Fengjing, Decoupling Control Based on PID Neural Network for Plasma Cutting System, *27th Chinese Control Conference*, 2008, 659-662.
- [12] Claudio H. Rivetta, Ali Emadi, Geoffrey A. Williamson, et al. Analysis and Control of a Buck DC-DC Converter Operating With Constant Power Load in Sea and Undersea Vehicles, *IEEE Trans. Ind. Application*, 42(2006), No.2, 559-572.
- [13] Suyong Chae, Byungchul Hyun, Pankaj Agarwal, et al. Digital Predictive Feed-Forward Controller for a DC-DC Converter in Plasma Display Panel, *IEEE Trans. Power Electron.*, 23(2008), No.2, 627-633.
- [14] Lucas T. N., Some Further Observations on the Differentiation Method of Model Reduction, *IEEE Trans. Automatic Control*, 37(1992), No.9, 1389-1391.

**Authors:** Baoqi Liu, 1037#, Luoyu Road, Huazhong University of Science and Technology, P.R.China, 430074, E-mail: liubaoqi1985@126.com.